

Article

# Numerical Calculation of Gas–Liquid Two-Phase Flow in Tesla Valve

Jie Gong, Guohua Li \*, Ran Liu and Zijuan Wang

Beijing Institute of Spacecraft Environment Engineering, Beijing 100094, China

\* Correspondence: li\_guohua@foxmail.com

**Abstract:** In this paper, the gas–liquid two-phase flow within a Tesla valve under zero-gravity conditions is numerically studied. Based on the VOF model and the inlet two-phase separation method, the forward and reverse flow patterns and pressure drop changes in a Tesla valve at different inlet velocities were analyzed. At an inlet velocity of 0.1–0.2 m/s, the flow pattern was slug flow, the bubbles were evenly distributed in different positions in the Tesla valve, and the velocity difference between the main pipe and the arc branch pipe was small. When the inlet velocity was 0.4 m/s, the main flow pattern was annular flow, and there was a phenomenon of gas–liquid phase separation through different flow channels, which was related to centrifugal force. At an inlet velocity of 0.6–0.8 m/s, bubbly flow and slug flow coexisted, which was related to the uneven velocity. In the study range, the difference in the forward and reverse pressure drops of two-phase flow was smaller than that of single-phase flow, and the two-phase diodicity decreased first and then increased with the change in inlet velocity, reaching minimum values of 0.78 at 0.2 m/s and 1.44 at 0.8 m/s.

**Keywords:** tesla valve; gas–liquid two-phase flow; flow pattern; pressure drop; diodicity



**Citation:** Gong, J.; Li, G.; Liu, R.; Wang, Z. Numerical Calculation of Gas–Liquid Two-Phase Flow in Tesla Valve. *Aerospace* **2024**, *11*, 409. <https://doi.org/10.3390/aerospace11050409>

Academic Editor: Hyun-Ung Oh

Received: 7 April 2024

Revised: 14 May 2024

Accepted: 15 May 2024

Published: 17 May 2024



**Copyright:** © 2024 by the authors. Licensee MDPI, Basel, Switzerland. This article is an open access article distributed under the terms and conditions of the Creative Commons Attribution (CC BY) license (<https://creativecommons.org/licenses/by/4.0/>).

## 1. Introduction

Gas–liquid two-phase flow has a high heat transfer capacity and is widely used in the aerospace field. It often appears in various heat pipes in spacecraft thermal control systems [1] and in the internal flow channels of various liquid nitrogen heat sinks, heat exchangers, and carburetors in space environment simulation equipment. With the development of new technologies, modern high-performance spacecraft use electronic chips with high integration, high power, and high heat flux, and need cooling technologies with a low weight, small volume, high heat transfer density, and high heat transfer efficiency [2–4]. With the development of new spacecraft, components with high heat flux have appeared in space environment simulation equipment, which requires corresponding high-efficiency thermal protection devices. These increasing demands put forward higher requirements on the heat dissipation capacity of traditional thermal control and thermal protection means. Therefore, one of the effective ways to improve the heat transfer performance is to study flow channels with new structures.

The Tesla valve was invented by the famous inventor Nikola Tesla [5]. Its forward pressure drop and reverse pressure drop are significantly different, so it can perform the function of a one-way valve by its internal structure. It plays a very important role in the field of microfluidic control and drive, so it is often called the “immovable micro-valve” in literature [6,7].

The internal flow of the Tesla valve is shown in Figure 1. In the forward flow, the fluid mainly flows through the main pipe, which is manifested as a high velocity in the main pipe and low velocity in the arc branch pipe. In the reverse flow, most of the fluid flows through the arc branch pipe, while a small part flows through the main pipe, and the impact at the interchange leads to greater resistance. This is because the arc branch pipe structure guides the fluid to the T-shaped connection, where it interferes with the main pipe fluid, thereby obstructing the reverse flow [6].

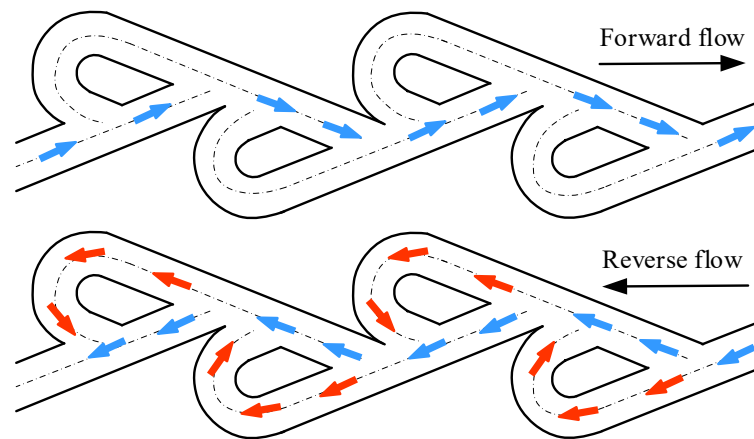


**Figure 1.** Forward flow and reverse flow of the Tesla valve.

In order to explore its internal mechanism and further improve its performance, many scholars have studied the optimization and improvement of its structural parameters. Ronald Louis Bardell [8] conducted theoretical and numerical studies on the internal mechanism of the Tesla valve, and proposed a key feature for characterizing the efficiency of the Tesla valve: diodicity, which means the ratio of the reverse pressure drop to the forward pressure drop. Bendib et al. [9] designed a new Tesla valve and conducted a numerical simulation using a turbulence model to study the influence of its structural parameters on the one-way flow efficiency. Turowski et al. [10] studied the transient characteristics inside the Tesla valve through the transient numerical simulation method and gave its equivalent circuit model. They called it a microfluidic diode based on the directional nature of the flow of the Tesla valve, which had similarities to diodes in the field of microelectronics. Thompson et al. [11] conducted a numerical study on a multistage Tesla valve and found the influence of parameters such as the number of stages and spacing on the rectification effect of the Tesla valve.

Xu et al. [12] redesigned the Tesla valve by means of topology optimization and obtained a high-efficiency Tesla valve with the inlet and outlet in the same direction. As shown in Figure 2, its shape is different from the traditional Tesla valve, but its internal mechanism is still basically the same as that of the Tesla valve.

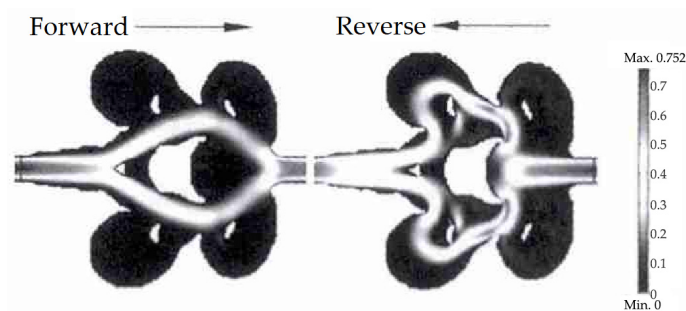


**Figure 2.** Topology-optimized Tesla valve structure [12].

F. K. Forster et al. [13,14] applied the Tesla valve to a valveless piezoelectric pump, as shown in Figure 3, and achieved good results. Wang Hao et al. [15] proposed a design scheme for a valveless piezoelectric pump based on inertial momentum action, and also adopted the Tesla valve as a valve without moving parts. Ivano Izzo et al. [16] used serial conical asymmetric resistance pipes, as shown in Figure 4, in their valveless piezoelectric pump, whose internal mechanism is still similar to that of the Tesla valve, but its structure is quite different, and there is no difference between the main pipe and the arc branch pipe.

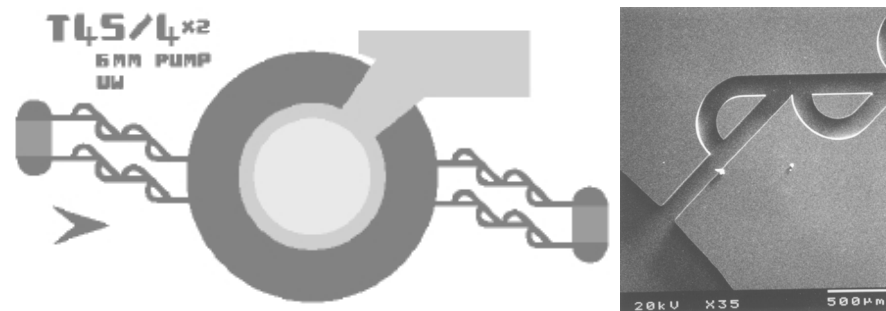


**Figure 3.** Application of Tesla valve in valveless piezoelectric pump [13,14].

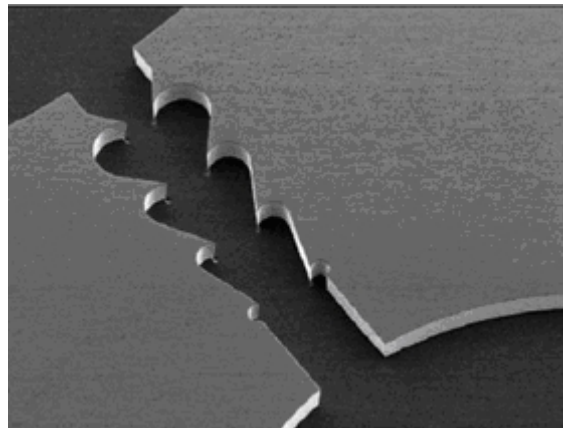


**Figure 4.** Conical asymmetric resistance tubes in tandem [16].

The one-way passage ability of the Tesla valve has also received strong attention in the field of gas–liquid two-phase flow. Thompson et al. [17] integrated the Tesla valve into the adiabatic section of a pulsating heat pipe to improve the overall thermal performance, as shown in Figure 5. They found that, compared with flat oscillating heat pipes without a Tesla valve, the use of a Tesla valve promoted circulation in the desired direction and that this boost increased with increasing heat input.

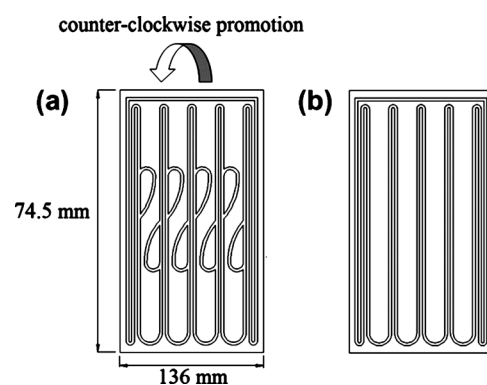


**Figure 5.** Application of Tesla valves in pulsating heat pipes (a) with Tesla valves (b) without Tesla valve [17].

De Vries et al. [18] designed a new type of Tesla valve and integrated it into the adiabatic section of the pulsating heat pipe to promote circulation, as shown in Figure 6. The study found that the velocity and thermal performance were improved after increasing the valve.

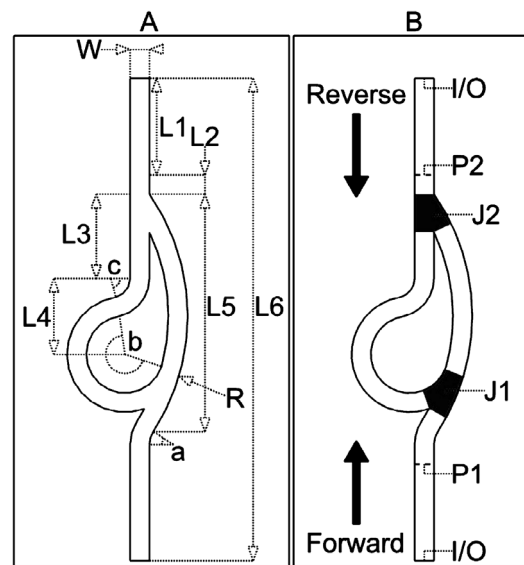


**Figure 6.** De Vries et al.'s modified Tesla valve (A,B) [18].

After an extensive literature search, it was found that the studies on gas–liquid two-phase flow in Tesla valves were mainly concentrated in the field of pulsating heat pipes, all were experimental studies, and no numerical calculation studies on gas–liquid two-phase flow in Tesla valves were found.

In this paper, the gas–liquid two-phase flow in the Tesla valve is numerically calculated using the VOF model, and the flow pattern distribution and resistance change rule in the Tesla valve under zero-gravity conditions are explored. It provides a technical basis for further improving the heat transfer capacity of two-phase systems.

## 2. Mathematical Models and Simulation Methods

### 2.1. Geometric Model and Mesh Generation

The calculation model, shown in Figure 7, is established according to the classic configuration that has been widely used today, namely the T45A Tesla valve structure mentioned in Ronald Louis Bardell's study [8].

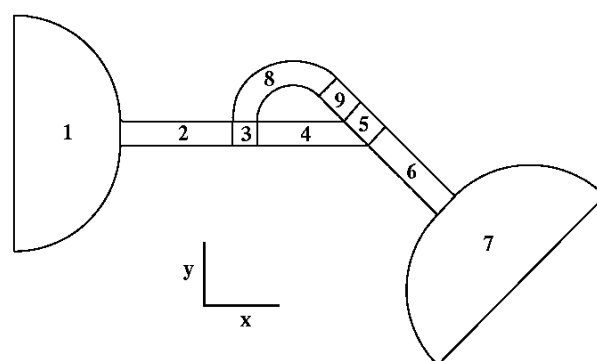


**Figure 7.** T45A Tesla valve structure mentioned in Ronald Louis Bardell's study, numbers indicate the area division [8].

The geometric model used for numerical calculation in this paper is shown in Figure 8. The geometric model is a two-stage series Tesla valve, and the structure of the Tesla valve is the classic T45A-type configuration. The angle of the arc side intersection is  $90^\circ$ , the angle of the linear side is  $45^\circ$ , and the flow channel section is a square with a side length of 2 mm. Due to the complex structure of the model, the calculation area is discretized by a tetrahedral unstructured mesh.

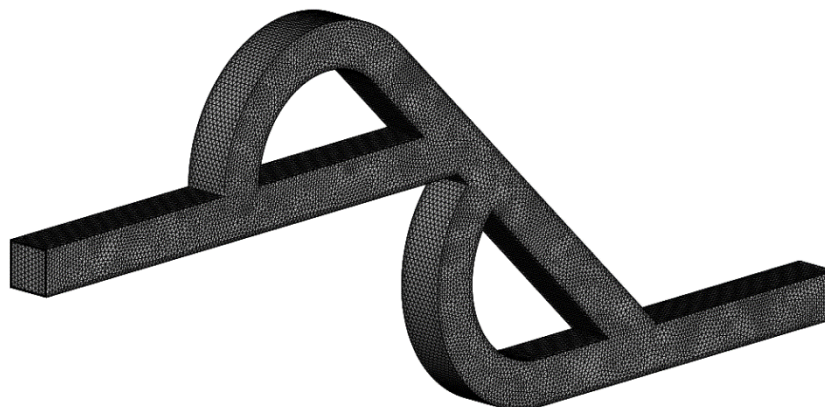


**Figure 8.** Geometric model and meshing diagram.

## 2.2. Mathematical Model

Since the gas phase and liquid phase are continuous phases, the Euler–Euler simulation method (two-fluid model) is adopted. The core of the method is to treat the mixture of different phases as interleaved continuous dielectric materials. Interface capture adopts the volume fraction model (VOF model). In the calculation process of this model, only a set of momentum equations are used by each phase flow fluid at the same time, and the volume fraction of each phase fluid in each control unit is obtained. Then, the velocity, temperature and pressure distribution of each phase flow fluid are obtained from the volume fraction.

The VOF method is an interface capturing technique that is well suited for simulating immiscible fluids with clearly defined interfaces, and is widely used in the scenario of flow pattern analysis, such as those observed in slug flow. In this flow regime, the gas and liquid phases are distinctly separated, and the VOF method can accurately track the evolution of the interface between them. However, it is important to note that the VOF method may not be the most appropriate choice for simulating dispersed bubbly flow, where the phases are interpenetrating and the interfaces are not clearly defined.

Despite this limitation, we chose to use the VOF method for all the flow patterns in our study, including the dispersed bubbly flow, due to its ability to handle high gas volume fractions and its computational efficiency. While the VOF method may not capture the detailed dynamics of the interpenetrating phases in the bubbly flow regime, it can still provide valuable insights into the overall flow behavior and pressure drop characteristics.

## 2.3. Boundary Conditions

The boundary conditions are as follows: the inlet is set as the velocity-inlet, the outlet is the pressure-outlet, the pressure is normal pressure, and the wall boundary adopts adiabatic and non-slip boundary conditions.

The two phases are set as follows: the internal liquid phase is pure water and the gas phase is water vapor. The evaporation and condensation process of the phase interface is considered in the calculation, and both the gas–liquid phases at the inlet are 100 °C. The thermo-physical properties of the liquid and gas phases used in our simulations are summarized in Table 1.

**Table 1.** Thermo-physical properties of the liquid and gas phases.

| Property                          | Water Liquid                   | Water Vapor                    |
|-----------------------------------|--------------------------------|--------------------------------|
| Density (kg/m <sup>3</sup> )      | 958.36 (100 °C)                | 0.5978 (100 °C)                |
| Viscosity (Pa·s)                  | $2.82 \times 10^{-4}$ (100 °C) | $1.22 \times 10^{-5}$ (100 °C) |
| Surface tension coefficient (N/m) | 0.0589 (100 °C)                | -                              |
| Evaporation temperature (°C)      | 100                            | -                              |
| Condensation temperature (°C)     | -                              | 100                            |

The gas content of the inlet (gas volume fraction) is set to 0.5. This parameter does not adopt the method of directly setting the gas content of the inlet two-phase flow, but separates the gas phase and liquid phase into two areas on the inlet section, and the gas liquid enters respectively at the same velocity. The area ratio of different areas is the gas–liquid ratio of the inlet. In this study, the area of the gas inlet is the same as that of the liquid inlet.

Considering the influence of the surface tension of the gas–liquid interface and referring to the actual flow pattern, the inlet area is set as a shape, as shown in Figure 9, with the central circular area being the gas phase and the surrounding area being the liquid phase.

In our numerical simulations, the gas phase is positioned in the center of the channel at the inlet boundary. This phase distribution pattern is adopted to mimic the common scenario in two-phase flow systems, where the gas phase is injected into the liquid phase through a central nozzle or orifice. Such an arrangement promotes the formation of a symmetric flow pattern and is often encountered in practical applications, such as in gas–liquid mixers or bubble columns. Furthermore, the central positioning of the gas phase at the inlet helps to minimize the influence of the wall on the initial phase distribution, allowing for a more unbiased investigation of the flow patterns that develop downstream. This setup also facilitates the comparison of our results with experimental studies and other numerical simulations that employ similar inlet conditions.

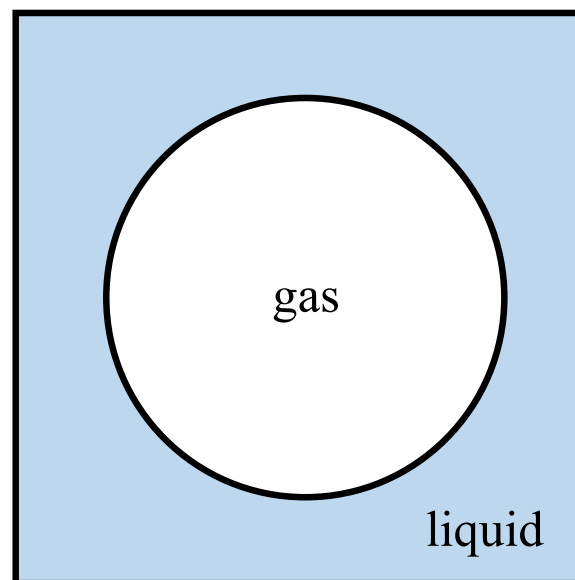


**Figure 9.** Liquid phase distribution in inlet breath.

### 3. Model Verification

The calculation model and boundary condition settings were verified using a 2 mm square cross-section straight tube. Numerical calculations were performed at inlet velocities of 0.1, 0.2, 0.4, 0.6 and 0.8 m/s, respectively. Figure 10 shows the calculated gas phase volume fraction, and the flow pattern in the tube can be visually seen through the gas phase distribution. At a low inlet velocity, the flow pattern is a typical slug flow. With the increase in inlet velocity, the bubbles gradually elongate and break, respectively showing annular flow and bubbly flow; bubbly flow is a state in which a large number of tiny bubbles are evenly distributed in the liquid phase. Due to the small size of the bubbles, it is beyond the resolution of this calculation and shown as a uniform two-phase mixing state. At the same time, it can be observed that these flow patterns are rapid-forming and do not require a long evolving forming section, so it can be considered that the inlet setting can quickly obtain different flow patterns.

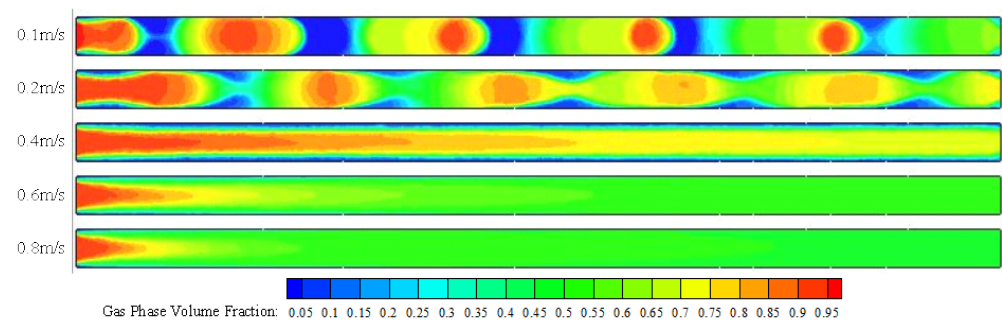


**Figure 10.** Flow pattern of gas–liquid two-phase flow in a straight pipeline at different inlet velocity values.

Figure 11 demonstrates the slug flow in the actual flow pattern [19,20]. By comparing Figure 10 with Figure 11, it can be observed that the flow pattern of the calculated results is accurate, and the model setting is deemed reasonable.

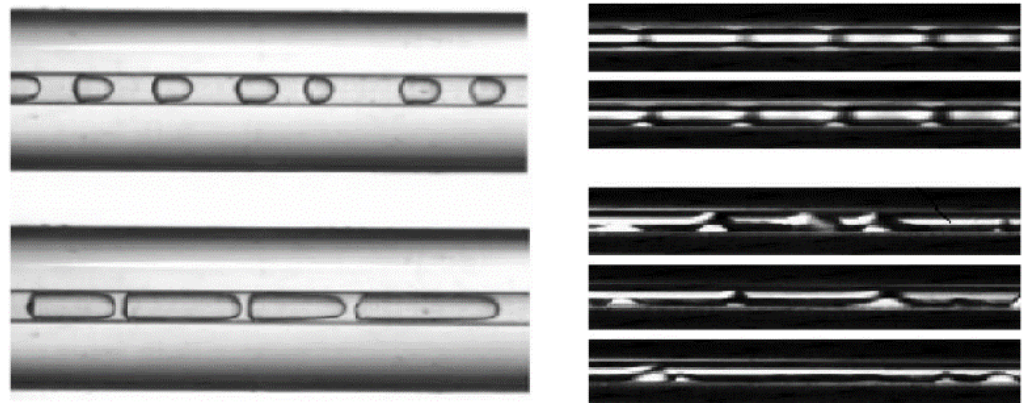


**Figure 11.** Slug flow in actual flow pattern [19,20].

## 4. Numerical Simulation Results

### 4.1. Two-Phase Flow Pattern

The two-phase flow patterns in different directions at different inlet velocities are obtained by numerical calculations for forward flow and reverse flow. The two-phase flow pattern in the Tesla valve has similar characteristics to that in the straight pipe, and its flow pattern is directly related to the inlet velocity, but because of the complexity of the flow channel, it also shows some unique phenomena.

#### 4.1.1. Slug Flow

At a low inlet velocity, the flow pattern is shown as slug flow. Figures 12 and 13 show the two-phase flow patterns in the Tesla valve at 0.1 m/s and 0.2 m/s flow velocities, respectively. As can be seen from the figure, the bubbles are evenly distributed in different positions within the Tesla valve, and the shapes of the bubbles are similar to each other, showing that the fluid flows through the main pipe and the arc branch pipe at similar velocities. The velocity nephogram shown in Figures 14 and 15 shows that the velocity difference between the main pipe and the arc branch pipe is not obvious, which is obviously different from the single-phase velocity shown in Figure 1. This is because the two-phase flow is affected by surface tension, which makes the slug bubble show greater resistance, thus reducing the difference between the main pipe and the arc branch pipe.

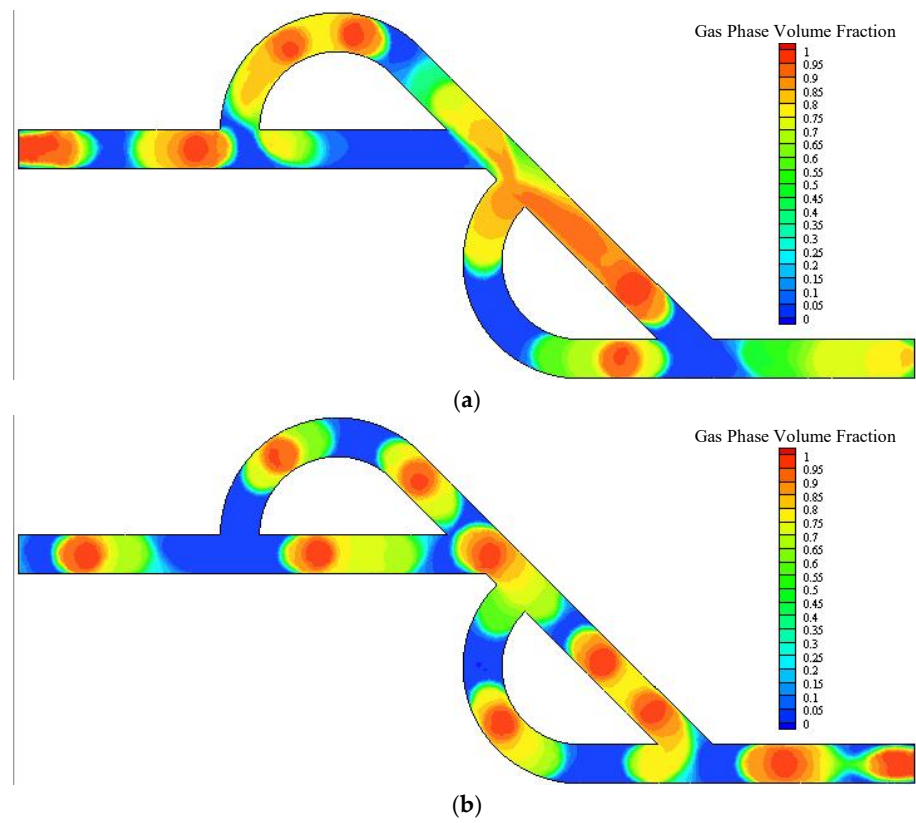


Figure 12. Two-phase flow pattern, inlet velocity 0.1 m/s. (a) Forward flow. (b) Reverse flow.

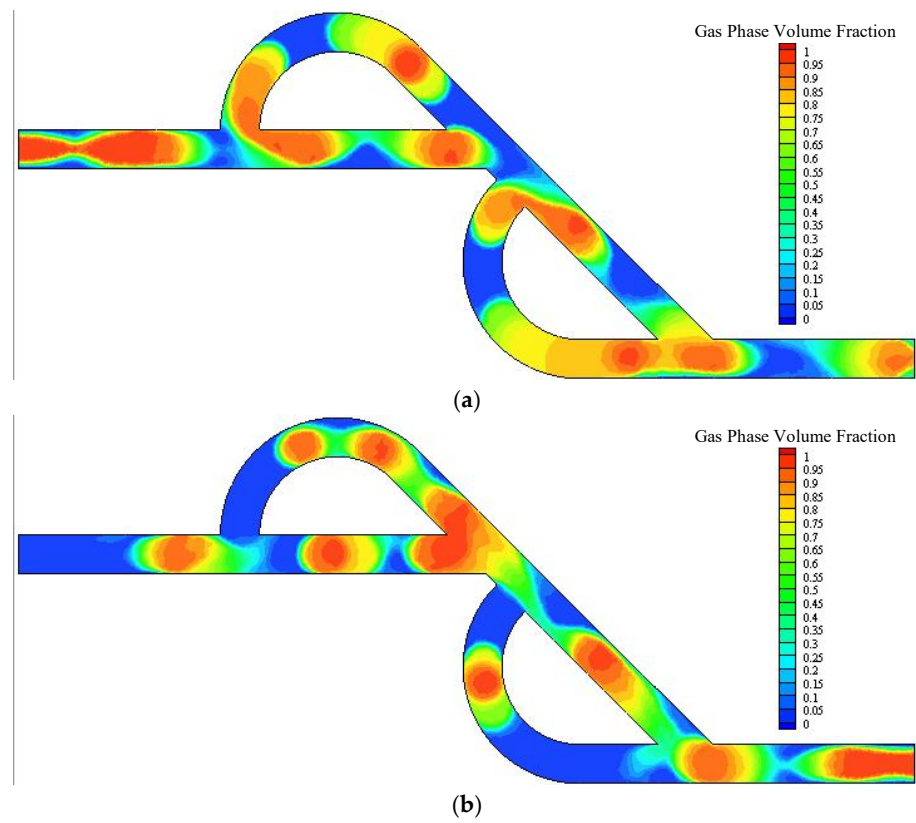


Figure 13. Two-phase flow pattern, inlet velocity 0.2 m/s. (a) Forward flow. (b) Reverse flow.

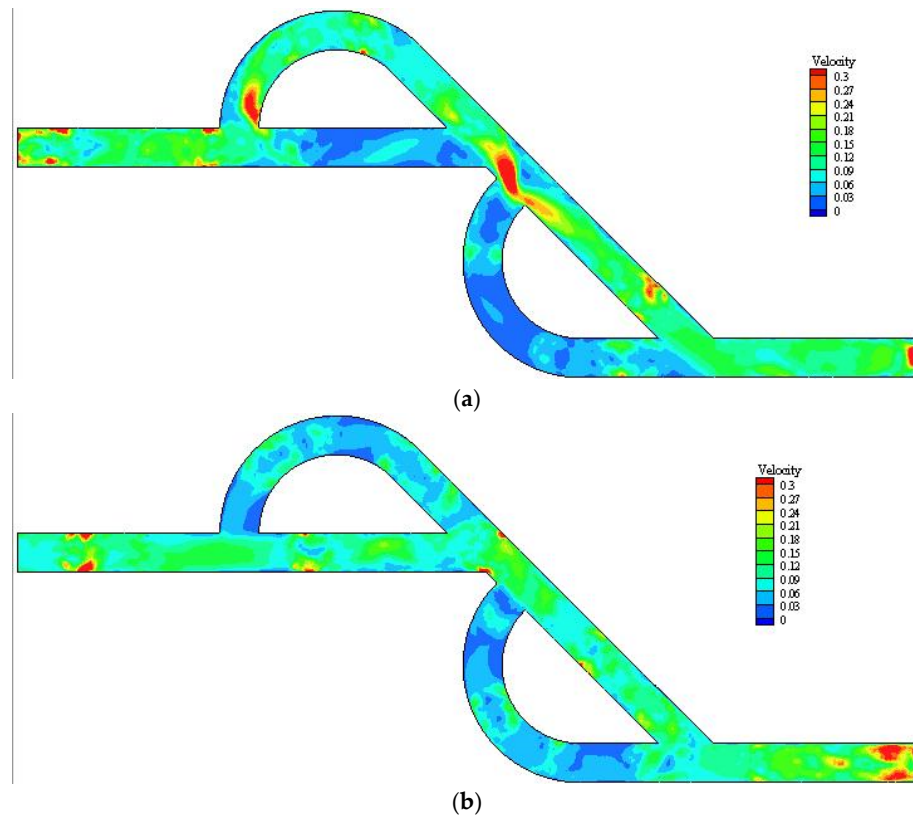


Figure 14. Velocity nephogram, inlet velocity 0.1 m/s. (a) Forward flow. (b) Reverse flow.

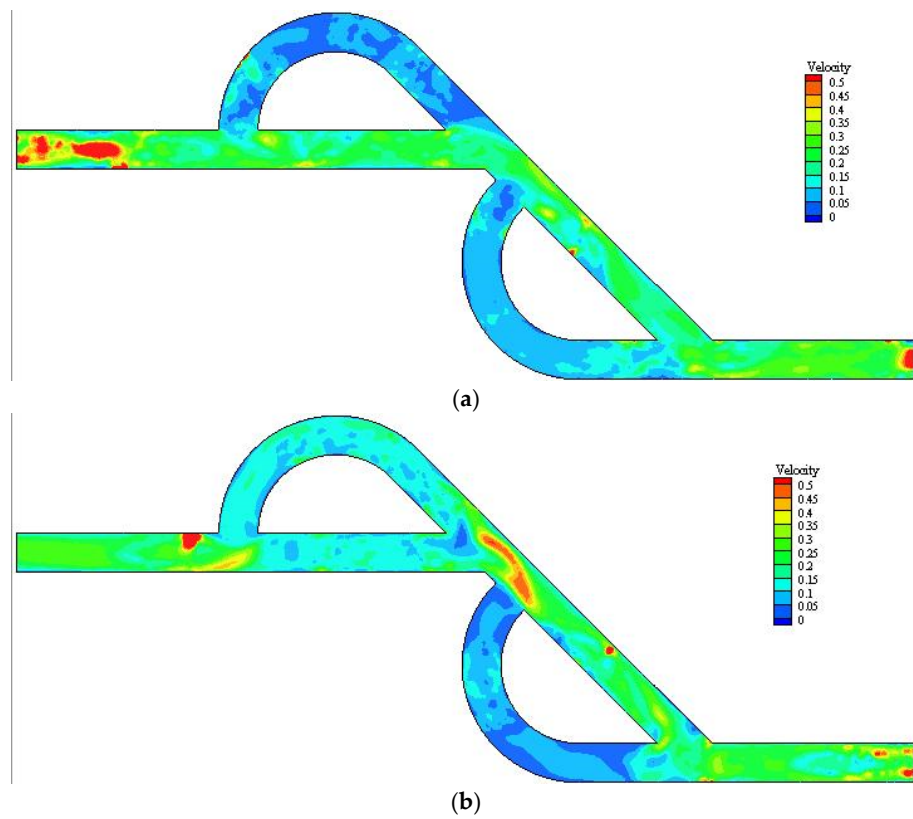


Figure 15. Velocity nephogram, inlet velocity 0.2 m/s. (a) Forward flow. (b) Reverse flow.

Figure 16 shows the flow pattern image obtained in the experiment of de Vries et al. [18], with an inlet velocity of 0.21 m/s. It shows that the flow pattern in the actual flow process was very close to the calculation results in this paper, which proves the calculation in this paper.



**Figure 16.** Two-phase flow pattern [18] in the experiment with an inlet velocity of 0.21 m/s.

#### 4.1.2. Annular Flow

Similar to the phenomenon in a straight pipe, when the inlet velocity is 0.4 m/s, the main flow pattern in the Tesla valve is annular flow, indicating that the liquid phase flows in a circular manner along the pipe wall and the gas phase is concentrated on the center line of the flow channel, forming a through-running path. The annular flow in the Tesla valve shows some unique phenomena; the gas–liquid phase is separated and flows through different flow channels, both in the forward flow and reverse flow, as shown in Figure 17. This gas–liquid separation is caused by centrifugal force; there is a flow line bending phenomenon at the main bend angle and the arc part of the straight pipe. The rotational motion brings a pressure gradient, thus causing a pressure difference on the surface of the bubble, forming a phenomenon similar to buoyancy, prompting the gas phase to deflate at a higher angle, resulting in the gas–liquid shunt phenomenon.

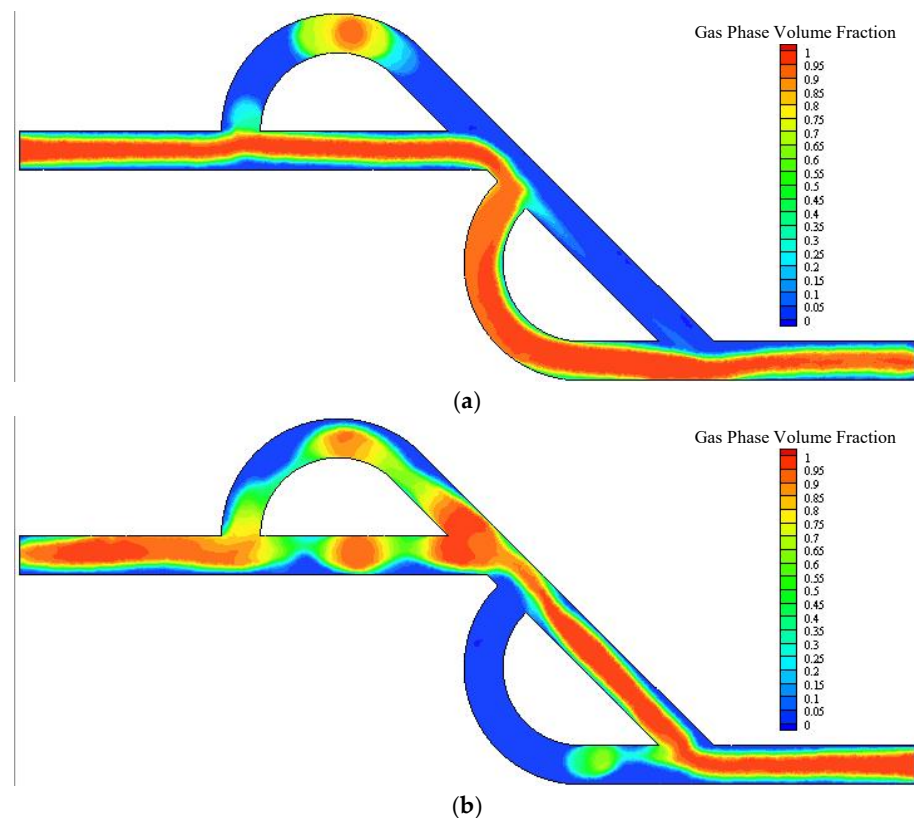


**Figure 17.** Two-phase flow pattern, inlet velocity 0.4 m/s. (a) Forward flow. (b) Reverse flow.

As the gas phase in the annular flow forms a pathway, the internal gas resistance is small, resulting in a higher velocity, which is very obvious in the velocity nephogram shown in Figure 18. It is worth noting that, because the gas density is low, the velocity is higher, but the mass flux is lower, so the velocity nephogram does not represent the flow path of most fluids.

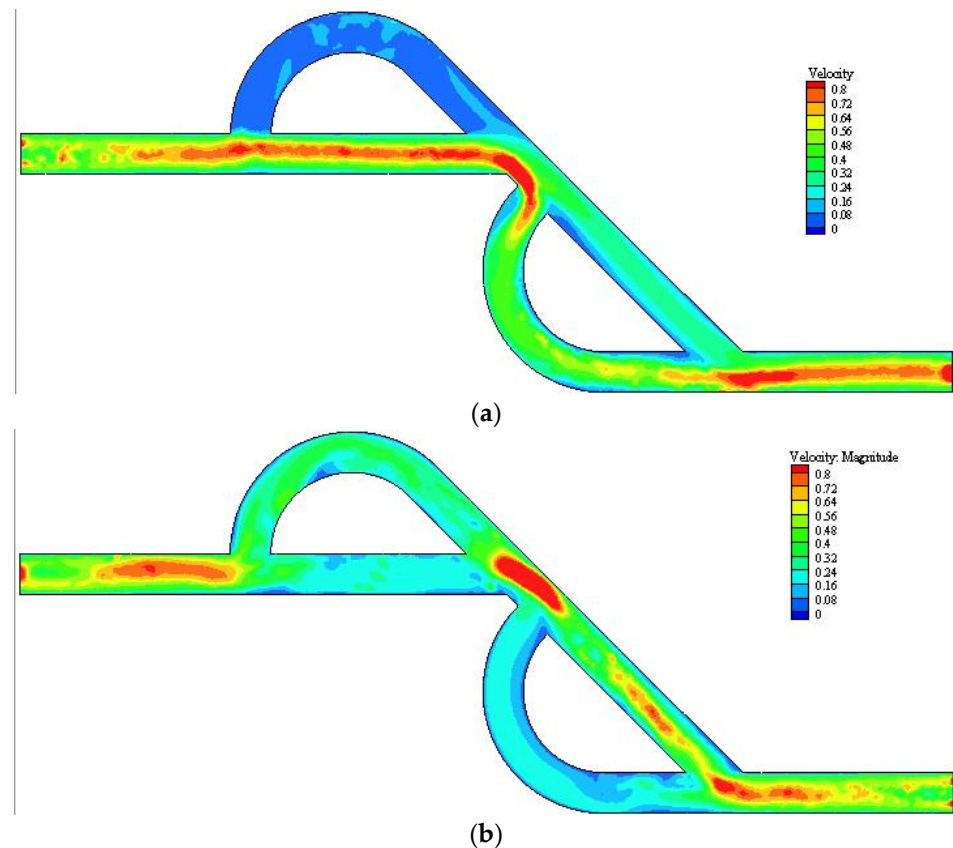


**Figure 18.** Velocity nephogram, inlet velocity 0.4 m/s. (a) Forward flow. (b) Reverse flow.

#### 4.1.3. Bubbly Flow

At higher inlet velocities, the inertial force is more dominant than the surface tension, and the larger bubbles break to form tiny bubbles or tiny droplets. These bubbles or droplets are small in size and the mesh density used for numerical calculations is not sufficient to capture their interfaces, so they are expressed as volume fractions within a single mesh.

Figures 19 and 20 show the flow pattern for inlet velocities of 0.6 m/s and 0.8 m/s, respectively. It can be found that, in the forward flow, the bubbly flow is mainly in the main pipe, and the arc branch pipe exhibits slug flow. In the reverse flow, the bubbly flow is concentrated in the arc branch pipe, and the main pipe of the second section exhibits obvious slug flow. According to the velocity nephogram analysis shown in Figures 21 and 22, it can be seen that the velocity is relatively small where the slug flow appears, and the velocity just meets the generation condition of the slug flow. The velocity nephogram has similar characteristics to that of single-phase flow, showing that when the inertia force is dominant, the flow characteristics are more similar to single-phase flow.

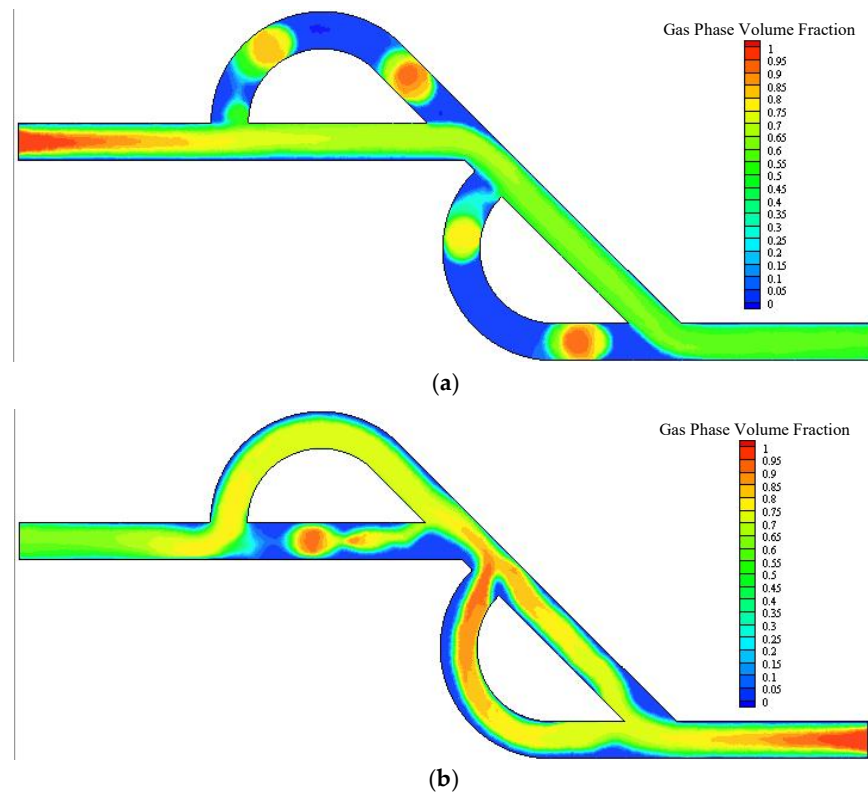


Figure 19. Two-phase flow pattern, inlet velocity 0.6 m/s. (a) Forward flow. (b) Reverse flow.

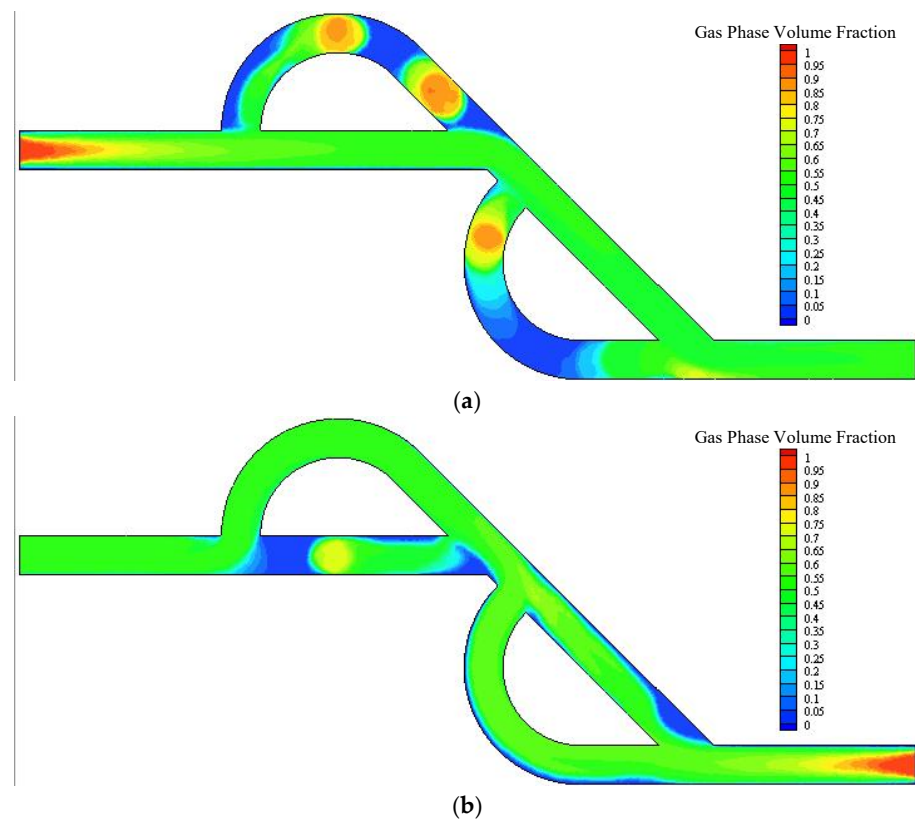


Figure 20. Two-phase flow pattern, inlet velocity 0.8 m/s. (a) Forward flow. (b) Reverse flow.

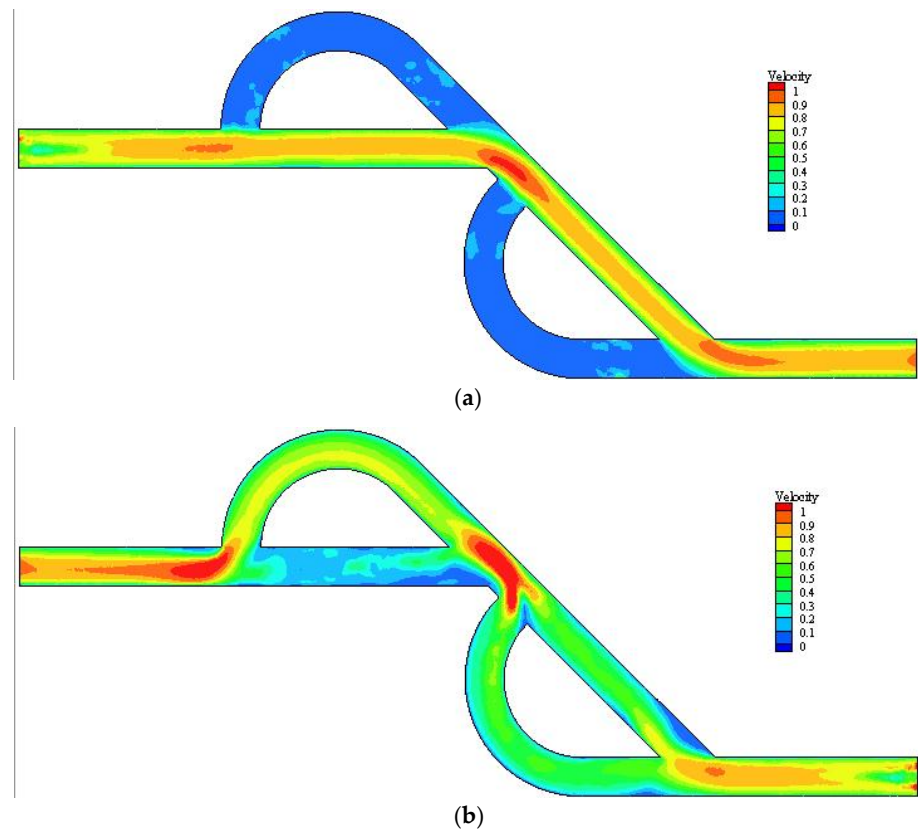


Figure 21. Velocity nephogram, inlet velocity 0.6 m/s. (a) Forward flow. (b) Reverse flow.

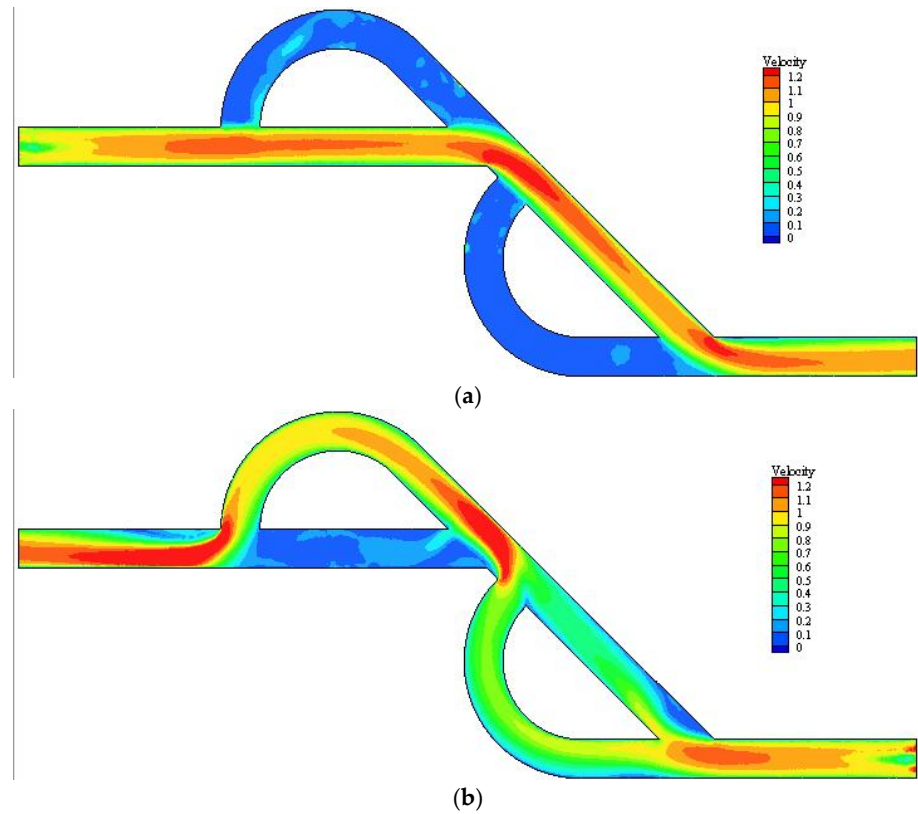


Figure 22. Velocity nephogram, inlet velocity 0.8 m/s. (a) Forward flow. (b) Reverse flow.

#### 4.2. Diodicity

In the process of numerical calculation in this paper, the outlet pressure is always normal pressure, and the average inlet pressure is taken as the pipeline pressure drop. The change curve of pressure drop can be obtained as shown in the left figure of Figure 23. The single-phase pressure drop as a contrast in the figure is obtained by numerical calculation of single-phase flow using the same geometric model. The diodicity is the ratio of reverse pressure drop to forward pressure drop, which is an important indicator of the one-way performance of Tesla valve. The pressure drop of the calculation example in this paper is shown in the right figure of Figure 23.

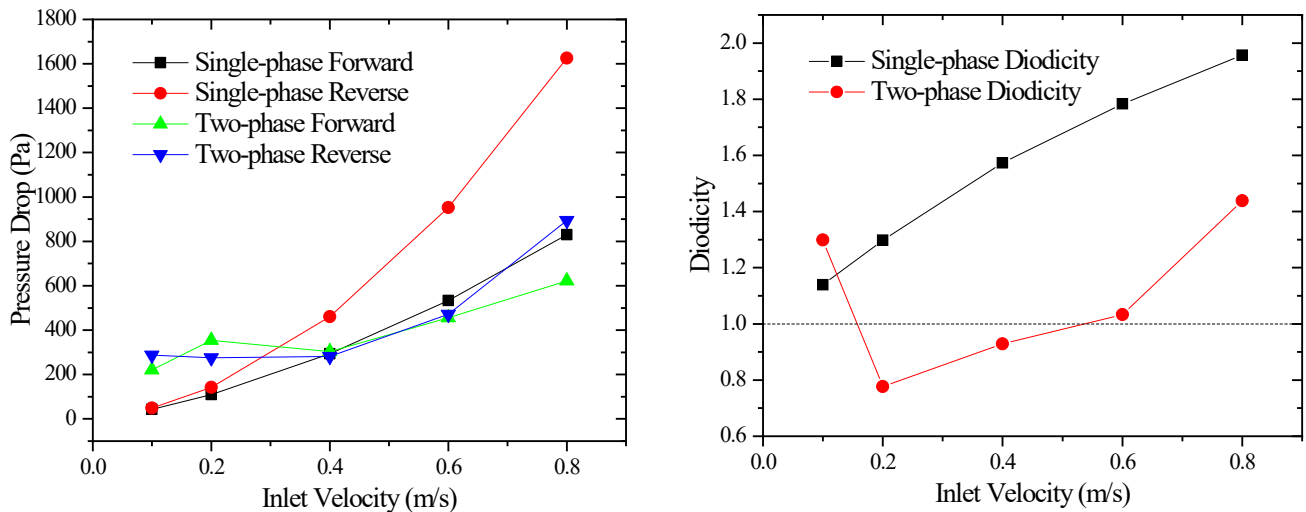


Figure 23. Pressure drop and diodicity change curve with inlet velocity.

It can be found that the single-phase reverse pressure drop is obviously larger than the single-phase forward pressure drop, and the gap increases with the increase of inlet velocity, so the diodicity also increases with the increase of inlet velocity. The two-phase pressure drop is obviously larger than the single-phase pressure drop at low inlet velocity, because the surface tension plays a dominant role at low inlet velocity, which causes the pressure drop to increase. In the inlet velocity of 0.2–0.4 m/s, the bubble breaks and forms an annular flow, and the pressure drop decreases slightly, forming a negative slope curve. Since then, the inertial force plays a dominant role, and the pressure drop gradually increases, whose value is close to the single-phase forward pressure drop, and there is no obvious difference between the forward and reverse directions. This makes the two-phases diodicity remain near to 1.0, and the minimum value is 0.78 at the inlet velocity of 0.2 m/s, and then the diodicity shows an increasing trend, reaching 1.44 at 0.8 m/s.

It is worth noting that the horizontal coordinate chosen here is the inlet velocity, which is convenient to compare the two-phase pressure drop with the single-phase pressure drop. Considering the density change caused by the gas content of two-phase flow, the mass flux is generally used to compare in engineering, which is more in line with the practical application requirements. Figure 24 shows the changes of pressure drop and diodicity with the mass flux. It can be seen that the two-phase pressure drop is significantly greater than that of the single-phase pressure drop with the same mass flux, which is consistent with the conclusions of previous studies in straight tubes.

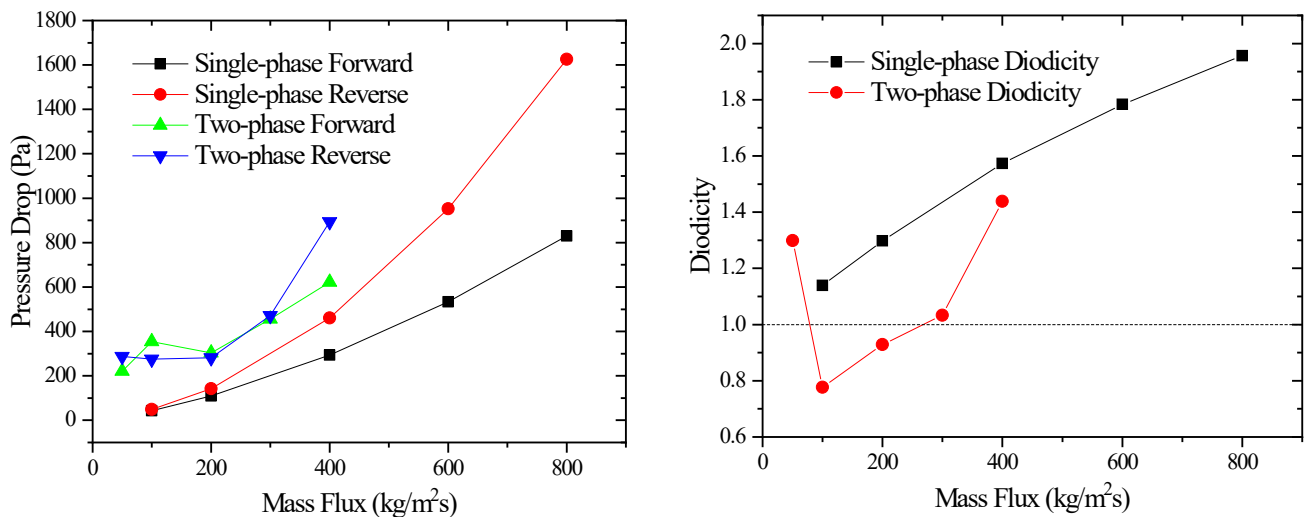


Figure 24. Pressure drop and diodicity change curve with mass flux.

## 5. Conclusions

In this paper, the gas–liquid two-phase flow in the flow passage of two Tesla valves under zero-gravity conditions with a rectangular section was numerically calculated. By using the VOF model and the inlet two-phase separation method, the forward and reverse flow patterns and pressure drop changes in the Tesla valves under different inlet velocities were analyzed. The main conclusions are as follows:

1. The flow pattern in the Tesla valve is related to the inlet velocity. At the low inlet velocity (0.1–0.2 m/s), the flow pattern is slug flow. The bubbles are distributed evenly at different positions in the Tesla valve, and affected by surface tension, the bubble resistance is large, resulting in a small difference between the velocity of the main pipe and the arc branch pipe.
2. When the inlet velocity is 0.4 m/s, the main flow pattern in the Tesla valve is annular flow and the gas–liquid phase separation flows through different flow channels, which is related to the pressure gradient generated by centrifugal force.
3. At a higher inlet velocity (0.6–0.8 m/s), bubbly flow and slug flow coexist. Due to the dominant role of inertia force, its flow characteristics are closer to single-phase flow, which generates different velocities at different locations, resulting in different flow patterns.
4. Within the study range, the difference in the forward and reverse pressure drops of two-phase flow was smaller than that of single-phase flow. The two-phase diodicity remained around 1.0, and decreased first and then increased with the change in inlet velocity, reaching minimum values of 0.78 at 0.2 m/s and 1.44 at 0.8 m/s.

Based on the simulated cases presented in this study, the use of Tesla valves in two-phase gas–liquid flow applications shows promise under certain flow regimes and operating conditions. Our simulations demonstrate that the unique geometry of the Tesla valve, with its alternating main and branch channels, can enhance mixing and separation between the gas and liquid phases and promote the breakup and coalescence of gas bubbles. In slug, annular, and bubble flows, the geometry of the Tesla valve appears to effectively regulate the flow pattern distribution, facilitate gas discharge, and improve the overall system performance. However, it is important to note that the effectiveness of Tesla valves in two-phase gas–liquid flows may be dependent on factors such as the specific valve geometry, flow rates, and fluid properties. Our study focused on a single Tesla valve geometry, and further investigations considering different valve designs and operating conditions are necessary to fully assess the feasibility and optimal application range of Tesla valves in these systems. Despite the limitations of our study, the results suggest that Tesla valves have the potential to offer advantages in certain two-phase gas–liquid flow applications.

The improved mixing and dispersion characteristics observed in our simulations indicate that Tesla valves merit further exploration and consideration as a viable flow control and enhancement device in these systems.

**Author Contributions:** Conceptualization, J.G. and G.L.; methodology, R.L.; validation, R.L. and Z.W.; formal analysis, R.L.; investigation, G.L.; resources, R.L.; data curation, G.L.; writing—original draft preparation, G.L.; writing—review and editing, J.G.; visualization, G.L.; supervision, J.G.; project administration, Z.W. All authors have read and agreed to the published version of the manuscript.

**Funding:** This research received no external funding.

**Data Availability Statement:** The raw data supporting the conclusions of this article will be made available by the authors on request.

**Conflicts of Interest:** The authors declare no conflict of interest.

## References

1. Li, D.; Liu, X.; Deng, W. Application of heat pipe technology in spacecraft thermal control. *Spacecr. Environ. Eng.* **2016**, *33*, 9.
2. Zhang, Y.; Chen, F.; Tian, F. Development on Heat Dissipation Technique of Airborne Electronic Equipment. *Aeronaut. Comput. Tech.* **2012**, *4*, 117–120.
3. Chen, E. The Heating Design Study of Electronic Equipment. *Refrigeration* **2009**, *3*, 59–64.
4. Yang, F. Research on the Thermal Analysis of PCB Circuit. *Power Electron.* **2011**, *45*, 91–92.
5. Nikola, T. Valvular Conduit. U.S. Patent 1329559, 3 February 1920.
6. Chen, C.; Shen, F.; Liu, Z. Analysis of Internal Flow Field and Research on Configuration Factors of Tesla Valve. In Proceedings of the China Mechanics Conference and the 100th Anniversary Commemorative Conference of Qian Xuesen's Birthday, Harbin, China, 22–24 August 2011.
7. Huang, J. *Theoretical and Experimental Research on Valveless Piezoelectric Pump with Flow Resistance Difference Tubes*; Nanjing University of Aeronautics and Astronautics: Nanjing, China, 2013.
8. Bardell, R.L. *The Diodicity Mechanism of Tesla-Type No-Moving-Parts Valves*; University of Washington: Seattle, WA, USA, 2000.
9. Bendib, S.; François, O.; Tabeling, P.; Willaime, H. Analytical study and characterization of micro-channel and passive micro-diode. In Proceedings of the 12th Micromechanics Europe Workshop, Cork, Ireland, 16–18 September 2001; pp. 147–150.
10. Turowski, M.; Chen, Z.; Przekwas, A. Automated generation of compact models for fluidic microsystems. *Analog Integr. Circuits Signal Process.* **2001**, *29*, 27–36. [[CrossRef](#)]
11. Thompson, S.M.; Paudel, B.; Jamal, T.; Walters, D.K. Numerical investigation of multistaged tesla valves. *J. Fluids Eng.* **2014**, *136*, 081102. [[CrossRef](#)]
12. Xu, Y.; Lin, S.; Den, Y. Research on Topology Optimization Design of Tesla-Type No-Moving-Parts Microvalves. *Comput. Simul.* **2014**, *31*, 373–376.
13. Forster, F.K.; Bardell, R.L.; Afromowitz, M.A.; Sharma, N.R.; Blanchard, A. Design, fabrication and testing of fixed-valve micro-pumps. *Asme Publ. Fed* **1995**, *234*, 39–44.
14. Forster, F.K.; Bardell, R.L.; Blanchard, A.P.; Afromowitz, M.A.; Sharma, N.R. Micropumps with Fixed Valves. U.S. Patent 5876187, 2 March 1999.
15. Wang, H.; Yao, H.; Du, C. A Micro-pump Based on the Hydro-inertia Effect. *Piezoelectr. Acoustoopt.* **2006**, *28*, 43–45.
16. Izzo, I.; Accoto, D.; Menciassi, A.; Schmitt, L.; Dario, P. Modeling and experimental validation of a piezoelectric micropump with novel no-moving-part valves. *Sens. Actuators A Phys.* **2007**, *133*, 128–140. [[CrossRef](#)]
17. Thompson, S.; Ma, H.; Wilson, C. Investigation of a flat-plate oscillating heat pipe with Tesla-type check valves. *Exp. Therm. Fluid Sci.* **2011**, *35*, 1265–1273. [[CrossRef](#)]
18. De Vries, S.; Florea, D.; Homburg, F.; Frijns, A.J.H. Design and operation of a Tesla-type valve for pulsating heat pipes. *Int. J. Heat Mass Transf.* **2017**, *105*, 1–11. [[CrossRef](#)]
19. Thome, J.R. Boiling in microchannels: A review of experiment and theory. *Int. J. Heat Fluid Flow* **2004**, *25*, 128–139. [[CrossRef](#)]
20. Liu, X.; Zhang, S.; Cheng, L.; Chang, W. Flow pattern transition criteria of flow boiling in confined mini/micro-channel. *CIESC J.* **2013**, *64*, 1573–1579.

**Disclaimer/Publisher's Note:** The statements, opinions and data contained in all publications are solely those of the individual author(s) and contributor(s) and not of MDPI and/or the editor(s). MDPI and/or the editor(s) disclaim responsibility for any injury to people or property resulting from any ideas, methods, instructions or products referred to in the content.